PHYSICAL REVIEW C **86**, 034310 (2012)

Prolate shape of ^{140}Ba from a first combined Doppler-shift and Coulomb-excitation measurement at the REX-ISOLDE facility

C. Bauer,[1,*] T. Behrens,[2] V. Bildstein,[2] A. Blazhev,[3] B. Bruyneel,[3] J. Butterworth,[4] E. Clément,[5] L. Coquard,[1] J. L. Egido,[6] A. Ekström,[7] C. R. Fitzpatrick,[8] C. Fransen,[3] R. Gernhäuser,[9] D. Habs,[9] H. Hess,[3] J. Leske,[1] T. Kröll,[1,2] R. Krücken,[2,10] R. Lutter,[9] P. Marley,[4] T. Möller,[1] T. Otsuka,[11,12] N. Patronis,[13,14] A. Petts,[4] N. Pietralla,[1,15] T. R. Rodríguez,[15] N. Shimizu,[12] C. Stahl,[1] I. Stefanescu,[13] T. Stora,[16] P. G. Thirolf,[9] D. Voulot,[16] J. van de Walle,[16] N. Warr,[3] F. Wenander,[16] and A. Wiens[3]

[1]*Institut für Kernphysik, Technische Universität Darmstadt, Darmstadt, Germany*
[2]*Physik-Department E12, Technische Universität München, Garching, Germany*
[3]*Institut für Kernphysik, Universität zu Köln, Köln, Germany*
[4]*Department of Physics, University of York, York, United Kingdom*
[5]*GANIL, Caen, France*
[6]*Departamento de Fisica Teorica, Universidad Autonoma de Madrid, Madrid, Spain*
[7]*Fysiska Institutionen, Lunds Universitet, Lund, Sweden*
[8]*Department of Physics, University of Manchester, Manchester, United Kingdom*
[9]*Fakultät für Physik, Ludwig-Maximilians-Universität München, Garching, Germany*
[10]*TRIUMF, Vancouver, Canada*
[11]*Department of Physics, University of Tokyo, Tokyo, Japan*
[12]*Center for Nuclear Study, University of Tokyo, Tokyo, Japan*
[13]*Instituut voor Kern- en Stralingsfysica, Katholieke Universiteit Leuven, Leuven, Belgium*
[14]*Department of Physics, University of Ioannina, Ioannina, Greece*
[15]*GSI Helmholtzzentrum für Schwerionenforschung GmbH, Darmstadt, Germany*
[16]*CERN, Genève, Switzerland*

(Received 16 July 2012; published 7 September 2012)

Background: Quadrupole moments of excited nuclear states are important observables for geometrically interpreting nuclear structure in terms of deformed shapes, although data are scarce and sometimes ambiguous, in particular, in neutron-rich nuclides.

Purpose: A measurement was performed for determining the spectroscopic quadrupole moment of the 2_1^+ state of ^{140}Ba in order to clarify the character of quadrupole deformation (prolate or oblate) of the state in its yrast sequence of levels.

Method: We have utilized a new combined technique of lifetime measurement at REX-ISOLDE and MINIBALL using the Doppler-shift attenuation method (DSAM) and a reorientation analysis of Coulomb-excitation yields.

Results: On the basis of the new lifetime of $\tau(2_1^+) = 10.4^{+2.2}_{-0.8}$ ps the electric quadrupole moment was determined to be $Q(2_1^+) = -0.52(34)$ eb, indicating a predominant prolate deformation.

Conclusions: This finding is in agreement with beyond-mean-field calculations using the Gogny D1S force and with results from the Monte Carlo shell-model approach.

DOI: 10.1103/PhysRevC.86.034310 PACS number(s): 21.10.Tg, 21.10.Ky, 21.60.Cs, 27.60.+j

I. MOTIVATION

The properties of the ground states and low-lying excited states of many atomic nuclei can be attributed to the correlated or collective motion of their nucleons in terms of surface oscillations or rotation of a permanently deformed spatial distribution. They reflect the structural changes when progressively more particles or holes are added to closed-shell nuclei, at first softening the (spherical) nuclear potential and then resulting in a deformed equilibrium shape.

The isotopic chain of the even-N Ba isotopes exhibits rather peculiar patterns of structural evolution. When neutrons are successively removed from the $N = 82$ neutron-shell closure, the collectivity of Ba isotopes increases and drives their shape from spherical toward considerabe deformation, passing a transitional region with soft triaxiality [1]. In the neutron-rich Ba isotopes with $N \geqslant 82$ the semimagic ^{138}Ba is spherical, whereas ^{148}Ba has a $R_{4/2} = E(4_1^+)/E(2_1^+)$ ratio of $\sim$2.98, closer to a deformed axially symmetric rotor. There is evidence for octupole correlations in the mass region around $A \sim 146$ ($Z = 56$, $N \sim 90$) that may influence the properties of nuclei already at low excitation energies since the resulting gain in binding energy is sufficient to stabilize permanent octupole deformations [2,3]. Still, low-lying energy levels with positive parity and electrical quadrupole transition probabilities of neutron-rich Ba isotopes have been successfully described throughout the transitional region in the framework of the Monte Carlo shell model based on a quadrupole-plus-pairing approach [4].

Indeed, in many nuclei deformation is predominantly of quadrupole nature [5]. Therefore a key observable to characterize the intrinsic nuclear shape in an even-even nucleus is the static quadrupole moment of the 2_1^+ state used in

*bauer@ikp.tu-darmstadt.de

conjunction with a collective model [6]. Together with the $E2$ transition rates it provides a sensitive tool for the study of spherical-to-deformed shape transitions. Since for lifetimes below ∼10 ns no direct method is available to determine the static quadrupole moment of excited nuclear states, the reduced electrical transition probabilities and lifetimes have to be used in order to obtain the spectroscopic quadrupole moment and nuclear deformation of these states [7].

In particular, the reorientation technique [8] can be used for the measurement of the spectroscopic quadrupole moment. It makes use of the fact that in Coulomb-excitation experiments, apart from the transitional matrix element $M_{20} = \langle 0_1^+ || M(E2) || 2_1^+ \rangle$ the cross section $\sigma(2_1^+)$ depends, to a smaller extent, also on the diagonal matrix element $M_{22} = \langle 2_1^+ || M(E2) || 2_1^+ \rangle$. The latter is related to the spectroscopic quadrupole moment: $Q(2_1^+) = 0.758 M_{22}$. Therefore, the Coulomb-excitation yield can be used for extracting information on the quadrupole moment $Q(2_1^+)$. The well known relation between the $B(E2)$ value and lifetime τ has then to be used to constrain the possible value of the M_{20} matrix element sufficiently precisely in such a Coulomb yield analysis. The importance of precise lifetime information as a *sine qua non* for the interpretation of data from reorientation experiments has been demonstrated recently when determining the sign of the spectroscopic quadrupole moment of the 2_1^+ state in ^{70}Se [9,10].

The uncertainty of the current literature value of $\tau = 14.0 \pm 5.9$ ps for the 2_1^+ state of ^{140}Ba [11] does not, however, permit this kind of analysis. Therefore a complementary lifetime measurement needs to be performed using the Doppler-shift attenuation method (DSAM). In order to efficiently use the precious beam time for intense radioactive beams and for minimizing systematical errors, it is desirable to do both measurements using the same setting of the radioactive beam. This approach differs from preceding experiments at MINIBALL applying the reorientation method with Coulomb-excitation reactions [9,12].

In this paper we will report on the measurement of the sign and magnitude of the spectroscopic quadrupole moment of the 2_1^+ state in neutron-rich unstable ^{140}Ba using a unique combination of the reorientation technique and the DSA method for the same setting of the radioactive beam.

II. EXPERIMENTAL DETAILS

Radioactive Ba isotopes were produced at the ISOLDE facility at CERN by bombarding a UC_x target with a 1.4 GeV proton beam. BaF^+ molecules were extracted to suppress the strong contamination from Cs. The BaF^+ molecules were trapped (REX-TRAP) and then cracked and Ba ions were charge-bred in the electron beam ion source (EBIS). A beam of ^{140}Ba ions was post-accelerated to an energy of 392 MeV (2.8 MeV/u) by the REX-Linac. A particle rate of about 10^5/s was available at the secondary target position. The ions were Coulomb-excited in two subsequent runs on a 0.9 mg/cm^2 ^{96}Mo target and on a 1 mm thick ^{nat}Cu target. The latter was thick enough for continuously slowing down the beam ions until they came to rest within the target. During the stopping

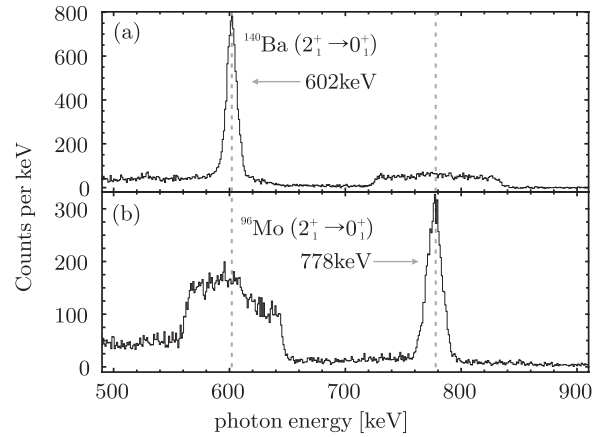

FIG. 1. Background-subtracted particle-γ coincidence spectra applying Doppler correction with respect to the (a) projectile or (b) recoiling target nuclei showing the only observed transitions, namely the $2_1^+ \rightarrow 0_1^+$ transitions in ^{140}Ba at 602 keV and in ^{96}Mo at 778 keV.

process the measured energies of the deexcitation γ rays of the ($2_1^+ \rightarrow 0_1^+$) transition of Coulomb excited ^{140}Ba ions are changed under the influence of the Doppler shift, resulting in a characteristic lineshape of the photopeak. All excited ions come to rest within 3 ps after their Coulomb excitation. The deexcitation γ rays were detected in the high-purity germanium cluster array MINIBALL covering about 2π of the solid angle [13]. The 20 HPGe crystals covered angles θ_γ between 43° and 77° and between 109° and 136°. In the case of the Mo target, the projectile- and target-like recoil ions were detected in forward direction in coincidence with the emitted γ rays in a double-sided silicon strip detector (DSSD) with an opening angle of $\theta_{lab} = 16.4°$–$54.2°$ [14].

Figure 1 shows the sum of the γ-ray spectra of all detectors of the MINIBALL array with Doppler correction for the Coulomb-excited ^{140}Ba projectiles (a) and ^{96}Mo target recoils (b) in coincidence with the particle signals from the DSSD. No γ-ray transitions other than the deexcitation of the 2_1^+ states to the ground states at 602 keV for ^{140}Ba and at 778 keV for ^{96}Mo were visible.

III. ANALYSIS AND RESULTS

A. DSAM analysis

In the present work a lifetime measurement was performed applying the Doppler-shift attenuation method. The lifetime of the 2_1^+ state of ^{140}Ba was deduced from individual DSAM fits for each of 18 crystals of the MINIBALL cluster detectors using the modified version of the program package LINESHAPE [15] of reference [16] and from a simultaneous fit to the 18 energy spectra using the newly developed program package APCAD [17].

From the individual fits, neglecting the angular distribution of the transition and the low-energy tail resulting from neutron damage, a first estimate for the lifetime of $\tau_{2_1^+}(^{140}\text{Ba}) = 12.5(6)$ ps was obtained. Then, the aforementioned effects have been included in the global fit using APCAD. In order to reproduce the low-energy tailing in the peak shapes due

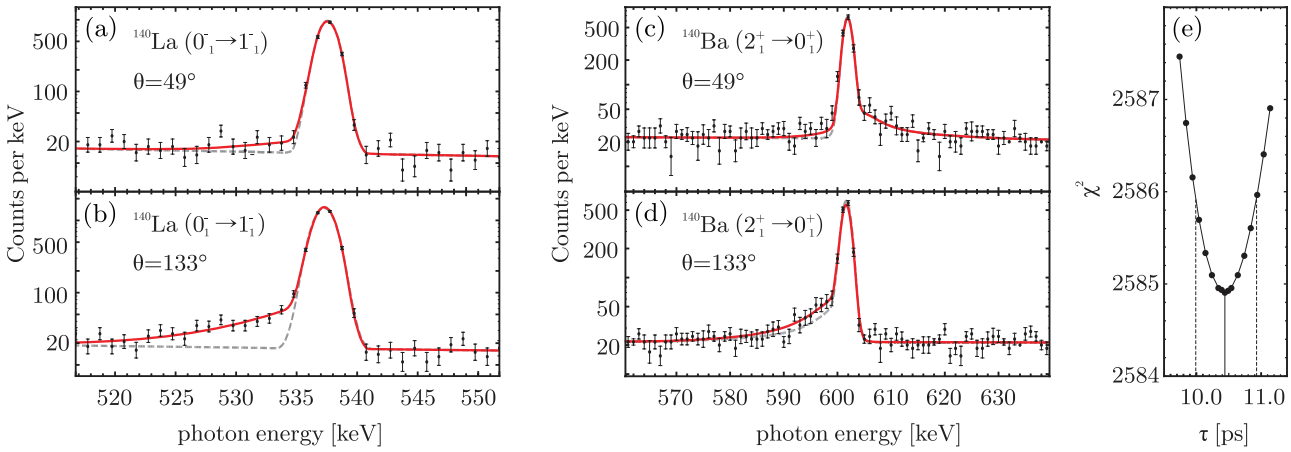

FIG. 2. (Color online) Panels (a) and (b) display the stopped $0^-_1 \rightarrow 1^-_1$ transition in ^{140}La from β decay of ^{140}Ba. Low-energy tails of the γ-ray lines appear due to partial neutron damage of the detectors. Dashed lines show a symmetric Gaussian peak shape compared to the fitted shape accurately, reproducing the described effect (solid). The Doppler-broadened lineshapes of the $2^+_1 \rightarrow 0^+_1$ transition in ^{140}Ba for (c) 49° and (d) 133° are shown after background subtraction. The spectra are shifted by $+20$ counts per channel for better visibility on the logarithmic scale. The full fits are represented by solid lines; the corresponding peak shapes without the effect of neutron damage are dashed. At forward angles the Doppler lineshapes are not significantly disturbed by any low-energy tailing due to partial neutron damage of the Ge detectors. Panel (e) shows the χ^2 values for the combined fit to the lineshapes detected in 18 crystals as a function of the lifetime of the 2^+_1 state ($\chi^2_{\mathrm{red,min}} = 0.92$).

to neutron damage, the detector response was modeled by a HYPERMET-like function from Ref. [18] and references therein. The parameters of the response functions have been determined individually for each crystal from a fit to the peak shape of the Doppler-free ($0^-_1 \rightarrow 1^-_1$) transition in ^{140}La at 537 keV following the β decay of ^{140}Ba. As a second major improvement compared to the LINESHAPE analysis, the influence of uncertainties of the stopping powers on the extracted lifetime has been quantified in a consistent way. The stopping matrices describing the Coulomb excitation and slowing-down process of the heavy ions in the target have been calculated from a Monte Carlo simulation based on the GEANT4 framework [19] using the stopping powers from Refs. [20–22]. The stopping powers have been varied by ±5% for the electronic stopping and ±20% for the nuclear stopping, thus reflecting their increasing uncertainty at low ion velocities. Examples for DSAM fits for one crystal in the forward direction and one crystal in the backward direction are shown in Figs. 2(c) and 2(d) together with the corresponding response functions fitted to the ($0^-_1 \rightarrow 1^-_1$) transition in ^{140}La. From the global fit a lifetime of

$$\tau_{2^+_1}(^{140}\mathrm{Ba}) = 10.4^{+2.2}_{-0.8}\ \mathrm{ps}$$

was obtained, in good agreement with the literature value but with significantly improved accuracy. With $^{+2.1}_{-0.7}$ ps the systematic uncertainties of the stopping powers clearly dominate the uncertainty of the final result. The statistical significance is demonstrated in Fig. 2(e).

B. Reorientation analysis

For the 2^+_1 state both the transitional and the diagonal matrix elements, M_{20} and M_{22}, affect the Coulomb-excitation cross section σ^P. Using the multiple Coulomb-excitation codes CLX and DCY [23] these matrix elements are varied such that the experimental γ yields (cf. Table I) are reproduced. The mutual dependency of σ^P on M_{20} and M_{22} results in a band in the (M_{22}, M_{20}) plane restricted by the required reproduction of the observed Coulomb-excitation cross section. The projectile excitation is normalized to the excitation σ^T of the 2^+_1 state of ^{96}Mo, taking also the angular distribution $W(\theta)$ of the γ rays into account by

$$\sigma^P(M_{20}, M_{22}) = \frac{N^P_\gamma}{N^T_\gamma}\frac{\epsilon^T}{\epsilon^P}\frac{W(\theta)^T}{W(\theta)^P}\sigma^T. \quad (1)$$

The main contributions to the uncertainty are the statistical errors of the experimental γ yields N_γ from projectile (^{140}Ba) and target excitation (^{96}Mo) as well as the uncertainty in the matrix elements of ^{96}Mo. The efficiency of the germanium detectors is denoted by ϵ and has an uncertainty of approx. 1%–2%. Figure 3 illustrates the increasing impact of the M_{22} matrix element on the differential Coulomb-excitation cross section as the scattering angle of the projectile-like recoils increases. This is best shown by the relative sensitivity

$$S = \frac{\sigma^P(M_{22} = +1.2M_{20}) - \sigma^P(M_{22} = -1.2M_{20})}{\sigma^P(M_{22} = 0)}, \quad (2)$$

defined as the relative variation of the cross section with the quadrupole moment ranging from prolate to oblate within the

TABLE I. Summary of the measured yields for the different ranges of scattering angles (not efficiency corrected).

Ring (DSSD)	θ_{lab} range	^{140}Ba	^{96}Mo
1 + 2	16.4°–22.9°	2717(55)	1442(39)
3 + 4	23.0°–28.9°	3089(59)	1759(43)
5 + 6	29.1°–34.3°	2465(52)	1453(39)

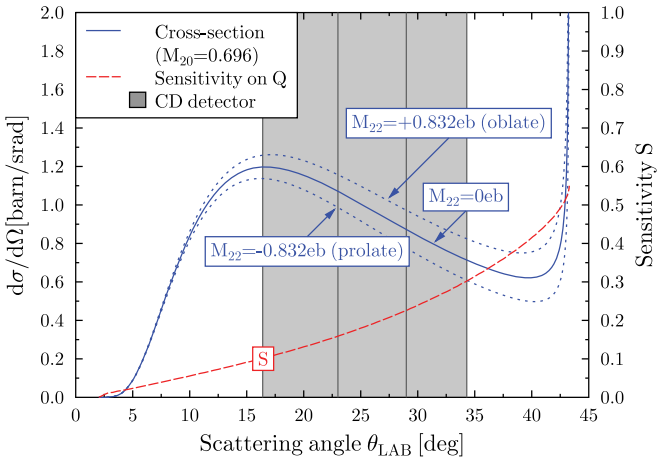

FIG. 3. (Color online) Differential Coulomb-excitation cross sections for the excitation of the 2_1^+ state in ^{140}Ba as function of the scattering angle in the laboratory frame for diagonal matrix elements $M_{22} = 0$ eb (solid curve) and for $M_{22} = \pm 0.832$ eb $= \pm 1.195 M_{20}$ which represent the rigid rotational limit for the M_{20} matrix element derived from the present lifetime. Each of the vertical bars (gray) illustrates the angular coverage of the corresponding rings of the CD detector. The relative sensitivity on Q is denoted by S [Eq. (2)].

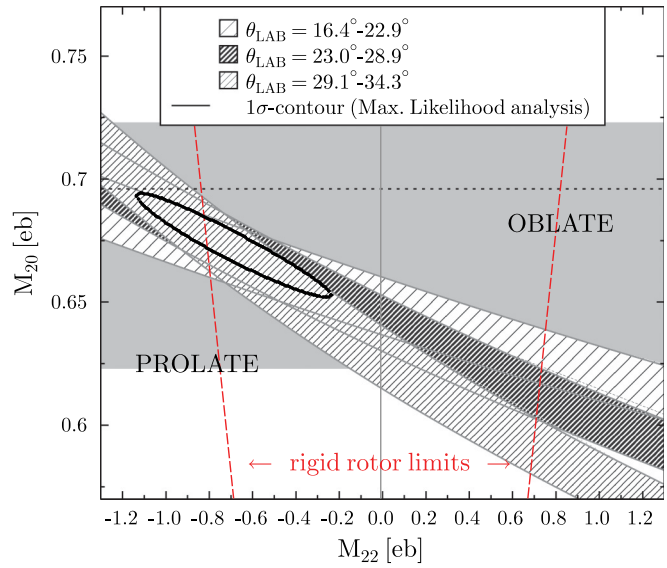

FIG. 4. (Color online) The bands for the different scattering-angle regimes show the agreement of the calculations with the experimental yields. The lifetime measurement provides the horizontal band as the allowed region of the transitional matrix element $\langle 2_1^+ || E2 || 0_1^+ \rangle$ (dashed line for the most likely value). Vertical dashed lines give the rotational model values ($M_{22} = \pm\ 1.195 M_{20}$) of a pure prolate or oblate rotor.

rigid rotational limit. In order to maximize the sensitivity to M_{22}, and related to this, to the quadrupole moment Q, three different scattering-angle ranges were defined. ^{140}Ba ions with scattering angles $\theta_{\rm lab} = 16.4°$–$22.9°$, $23.0°$–$28.9°$, and $29.1°$–$34.3°$ have been selected that correspond to two rings of the DSSD in each case.

A maximum-likelihood analysis (see Ref. [12]) finally yields a spectroscopic quadrupole moment of

$$Q(2_1^+) = -0.52(34)\ e\text{b}.$$

In Fig. 4 the contour curves in the (M_{22}, M_{20}) plane from the analysis of the experimental Coulomb-excitation yields and the lifetime analysis are shown. In addition, the results are summarized in Table II. The normalization to the target excitation [Eq. (1)] introduces also a dependency on the matrix element $M_{22} = \langle 2_1^+ || E2 || 2_1^+ \rangle$ of ^{96}Mo from which two different values, $M_{22} = +0.05(10)$ eb and $M_{22} = -0.26(11)$ eb, are reported in the literature [24]. The usage of the positive but small value of $M_{22} = +0.05(10)$ eb in the analysis of the present work would drive the quadrupole moment of ^{140}Ba beyond the limits of the rigid rotor. This finding is supported by a recent measurement of $Q(2^+)$ in ^{96}Mo yielding a negative diagonal matrix element of $-0.44(5)$ eb [25]. Therefore a weighted average of the two negative values for M_{22} is used in the analysis.

Due to the low beam energy at ≈65% of the Coulomb barrier, no transitions other than the ($2_1^+ \rightarrow 0_1^+$) one were observed. However, the influence of higher-lying states, namely the two-phonon states 2_2^+ and 4_1^+, has been considered as well in the Coulomb excitation calculation for an accurate estimate of experimental uncertainties of the results. To that end the unknown $E2$ matrix elements of the transitions ($4_1^+ \rightarrow 2_1^+$) and ($2_2^+ \rightarrow 2_1^+$) have been chosen such that the corresponding photopeaks would just meet the sensitivity limit given by the γ background in the spectrum. Further corrections result from the population of the 2_1^+ state via the 2_2^+ state, which gives rise to an interference term $P_3(2_1^+) = \langle 0_1^+ || M(E2) || 2_1^+ \rangle \langle 2_1^+ || M(E2) || 2_2^+ \rangle \langle 0_1^+ || M(E2) || 2_2^+ \rangle$ [26]. The influence of this interference is small (≈5%–10%) for the used beam energy but was considered in the analysis as well.

TABLE II. Comparison of experimental results for the transition $2_1^+ \rightarrow 0_1^+$ with theoretical calculations. The previously measured value is indicated by "Literature" and published in Ref. [11]. "Theory" values belong to Monte Carlo shell-model calculations [4] and EDF calculations including beyond-mean-field effects.

Nucleus	Experiment				Literature	Theory	
	τ	Matrix elements		$B(E2)\uparrow$, Q_s	$B(E2)\uparrow$, Q_s	$B(E2)\uparrow$, Q_s	
	(ps)	M.E.	(eb)	(e^2b^2), (eb)	(e^2b^2), (eb)	MCSM	EDF
^{140}Ba	$10.4^{+2.2}_{-0.8}$	$\langle 2_1^+ \|\| E2 \|\| 0_1^+ \rangle$	$0.696^{+0.027}_{-0.073}$	$0.484^{+0.038}_{-0.101}$	0.45(19)	0.33	0.594
		$\langle 2_1^+ \|\| E2 \|\| 2_1^+ \rangle$	−0.69(45)	−0.52(34)	n.m.	−0.51	−0.522

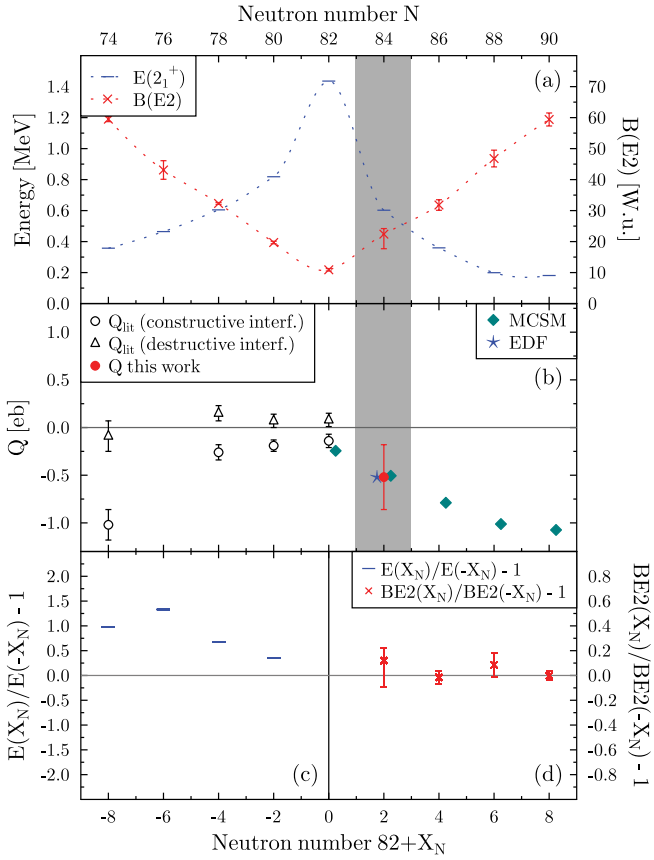

FIG. 5. (Color online) Systematics of excitation energy and $B(E2)$ value in W.u. (a) and Q moment (b) for the first excited 2_1^+ states in the even Ba isotopes with $130 \leqslant A \leqslant 146$. The ratio $E(2_1^+; 82 - X_N)/E(2_1^+; 82 + X_N) - 1$ is shown (c) and analogously $B(E2; 82 + X_N)/B(E2; 82 - X_N) - 1$ (d) to highlight the specific mirror symmetry of the transition strengths around $N = 82$. All $B(E2)$ values are given in W.u. in order to account for a simple size effect.

For the 2_2^+ state also the sign of the connecting matrix element has been varied (constructive and destructive interference). These effects have been included in the estimate of the experimental uncertainty of $Q(2_1^+)$ given above. They do not affect the conclusion on a predominant prolate deformation of the 2_1^+ state.

IV. DISCUSSION

A. Systematics

Experimental results are summarized in Table II and compared to predictions from our energy density functional (EDF) calculation and results from the Monte Carlo shell model (MCSM) [4]. The new lifetime $\tau(2_1^+) = 10.4^{+2.2}_{-0.8}$ ps in ^{140}Ba with significantly improved accuracy over the current literature value [11] corresponds to a $B(E2)\uparrow$ value of $0.484^{+0.038}_{-0.101} e^2b^2$. This is close to the B(E2;$0_1^+ \rightarrow 2_1^+$) value of 0.412(8) e^2b^2 in ^{136}Ba which is the neutron particle-hole partner nucleus to ^{140}Ba with respect to the $N = 82$ shell closure. The new result affirms the observation of a distinct symmetry in the electrical transition probabilities of the first excited states in the even-A Ba isotopes with respect to the $N = 82$ shell closure (see Fig. 5). In particular, the irregular pattern for the 2_1^+ excitation energies and $B(E2)\uparrow$ values discovered in the $N = 82$ particle-hole partners ^{130}Sn–^{134}Sn and ^{132}Te–^{136}Te [27] attributed to a reduced neutron pairing gap in the latter isotopes [28] does not exist in their nearby isotones ^{136}Ba–^{140}Ba. The electrical transition probabilities in the even-even Ba isotopes exhibit instead an astonishing symmetry around $N = 82$. This is in contrast to the evolution of the excitation energies, $E(2_1^+)$, as a function of neutron number. For those one observes a considerable asymmetry around $N = 82$, where the ratio $E(N = 82 - X_N)/E(82 + X_N)$ deviates from unity by up to 150% [Fig. 5(c)]. The different structure of Ba isotopes above and below the $N = 82$ shell closure is also emphasized by the evolution of the quadrupole moments, $Q(2_1^+)$, as shown in Fig. 5(b).

B. Monte Carlo shell-model calculations

The slightly prolate average deformation of the 2_1^+ state of ^{140}Ba with a spectroscopic quadrupole moment of $Q(2_1^+) = -0.52(34)$ eb confirms remarkably well the predictions of Monte Carlo shell-model calculations and the energy density functional (EDF, see below). The former, using a two-body effective interaction including monopole and quadrupole pairing, quadrupole-quadrupole interactions, and axially symmetric bases, describes microscopically the evolution of properties of quadrupole collective states throughout the shape transition path from ^{138}Ba to ^{150}Ba [4] with the variation of valence particles only. Although the calculated $B(E2)\uparrow$ value in ^{140}Ba is smaller than our experimental result, the spectroscopic quadrupole moments are in excellent agreement. The corresponding level scheme in Fig. 6(c) agrees quite well with the experimental one in Fig. 6(b), including the moment of inertia and the inverted order of the 0_2^+ and 2_2^+ states. The agreement of the yrast level schemes is slightly improved in comparison to Fig. 1(a) of Ref. [4] by including the triaxial degree of freedom.

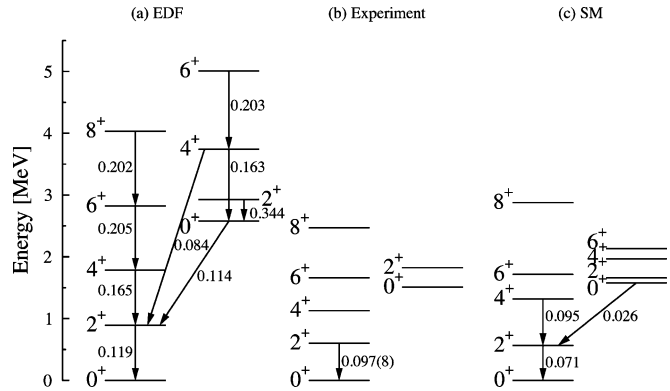

FIG. 6. (a) Energy levels calculated with the Gogny D1S density functional including beyond-mean-field effects. (b) Experimental level energies taken from Ref. [37] and $B(E2)\downarrow$ from this work. (c) Exact shell-model (SM) calculations using the $P + QQ$ interaction from the MCSM [4].

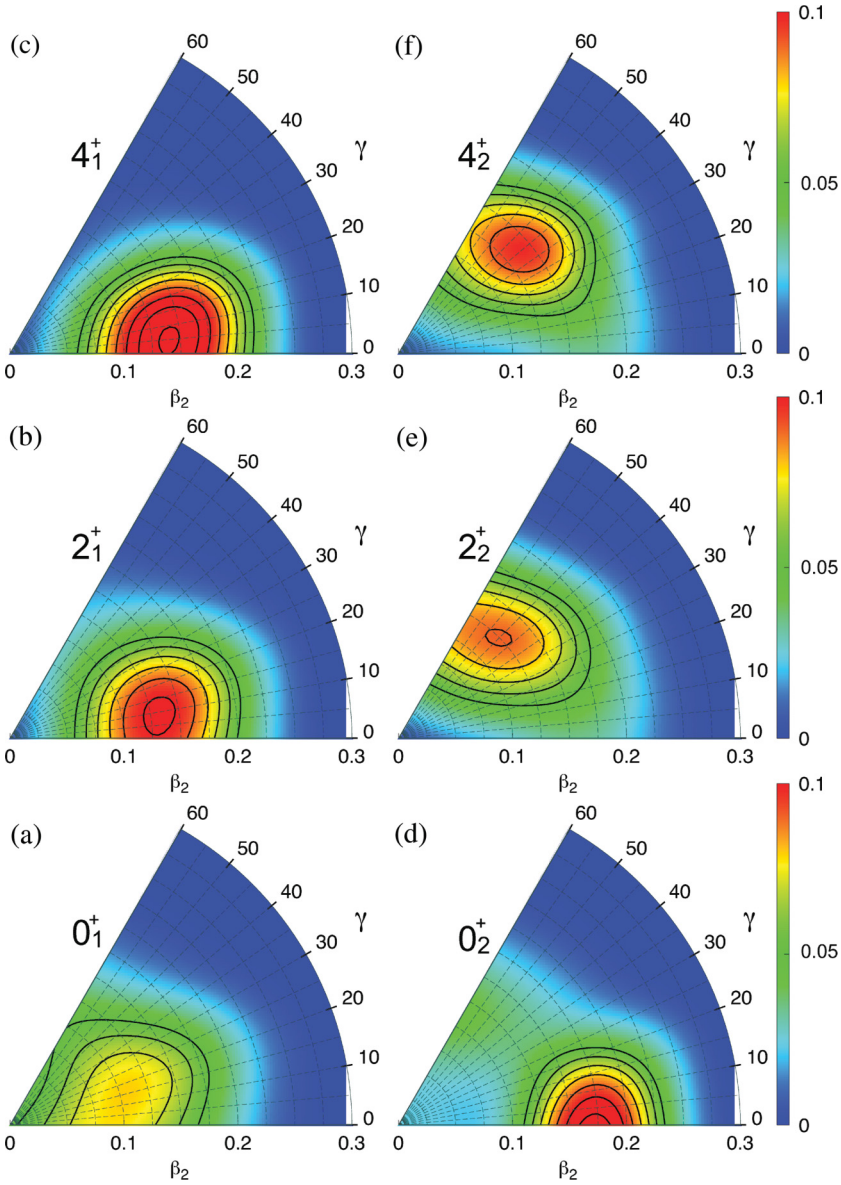

FIG. 7. (Color online) Distribution of probability in the triaxial (β_2, γ) plane (γ in degrees) for the states belonging to the first two bands calculated with the Gogny D1S density functional including beyond-mean-field effects.

C. Energy density functional

In order to obtain a more detailed understanding of the intrinsic deformation of the ground-state band and low-energy structure of ^{140}Ba, we have applied state-of-the-art energy density functional (EDF) methods based on the Gogny D1S functional [29] to compute the spectrum and reduced transition probabilities of ^{140}Ba. These techniques are suitable to study the intrinsic quadrupole deformations of the system (β_2, γ) because these degrees of freedom are taken into account explicitly in the calculations in a self-consistent manner. More details about these methods can be found in Refs. [30,31] and therein.

The two major limitations of the model used here are the conservation of parity and time-reversal symmetries of the intrinsic wave functions. The first one restricts the study to positive-parity states and neglects the influence of the octupole degree of freedom that could play a role in this region. However, axial mean-field calculations with the Gogny interaction show that octupole static deformations are not found in the potential energy surface for this specific isotope [32–34]. The second restriction limits the description of the moments of inertia and, therefore, the quantitative precision of the energy levels [35,36].

In Fig. 6(a) the results of the calculated spectrum are shown. These levels are sorted in bands according to their $B(E2)$ values. It is observed that the ground-state band corresponds to a sequence of states with positive parity and $\Delta J = 2$ almost equally spaced representative of a vibrational character. The second band is also compatible with a vibrational band for the levels 2_2^+, 4_2^+, and 6_2^+. However, the band head does not correspond to the 0_2^+ state which is higher in excitation energy than the 2_2^+ state. It is important to note that the correct ordering of these levels is only reproduced if the triaxial degree of freedom is included. The experimental levels also show a vibrational ground-state band, and the 2_2^+ state is below the 0_2^+ state. Nevertheless, although a good qualitative description of the data is obtained, the theoretical spectrum

appears more stretched. This is a common feature of this kind of method and is due to a poor description of the moments of inertia whenever the time-reversal symmetry is conserved, as in the present case [36]. Concerning the reduced transition probabilities, the calculation predicts that the 0_2^+ state decays mainly to the 2_2^+ state and the latter one to the 2_1^+ state, both possibly indicating pronounced γ softness. It is also observed that the calculated $B(E2, 2_1^+ \rightarrow 0_1^+)$ value is higher than the experimental value obtained in this work. It is important to mention that no effective charges are used in these methods.

We now analyze the intrinsic shapes of the states given in the spectrum, studying their corresponding collective wave functions. In Fig. 7 the distribution of probability of having a given deformation in the (β_2, γ) plane for different states J_σ^+ is shown. In the figure, the vertex corresponds to the spherical point, the $\gamma = 0^\circ$ and 60° directions correspond to prolate and oblate axially symmetric shapes respectively, and the rest of the plane corresponds to purely triaxial shapes. Here one sees clearly that the ground state presents a slightly deformed configuration $\beta_2 \sim 0.1$ with substantial γ softness, and the 2_1^+ and 4_1^+ states belonging to this band have their probabilities peaked at a larger, more prolate deformed shape around $\beta_2 \sim 0.13$, $\gamma = 5^\circ$; similar distributions are also obtained for 6_1^+ and 8_1^+ states (not shown). On the other hand, the first excited 0_2^+ state presents a maximum at $(\beta_2 = 0.17, \gamma = 0^\circ)$ while the 2_2^+ and 4_2^+ states show maxima located in the oblate-triaxial part at $(\beta_2 = 0.13, \gamma = 45^\circ)$. The differences and similarities between the corresponding collective wave functions help us to understand the values of the transition probabilities given in Fig. 6. In addition, this result is in agreement with the most probable prolate character of the 2_1^+ state found experimentally (Fig. 4).

V. SUMMARY AND CONCLUSION

In the present work we have presented results of a combined analysis of a DSAM lifetime measurement and of the reorientation technique in Coulomb excitation of a radioactive nucleus, for the measurement of the spectroscopic quadrupole moment of the 2_1^+ state in unstable neutron-rich ^{140}Ba. With the new lifetime $\tau(2_1^+) = 10.4^{+2.2}_{-0.8}$ ps, a prolate deformation was obtained, indicated by a quadrupole moment $Q(2_1^+) = -0.52(34)\ e$b. The result agrees with predictions from Monte Carlo shell-model calculations and state-of-the-art energy density functional methods. Both theoretical approaches reproduce the experimentally deduced deformation of ^{140}Ba without the incorporation of octupole correlations. From this one may infer that octupole correlations are insignificant for the properties of the 2_1^+ state of ^{140}Ba. It has been pointed out that the choice of axial or nonaxial symmetry in the Monte Carlo shell-model calculation has only little impact on the calculated Q moments of ^{138}Ba and ^{140}Ba [4]. However, triaxial deformation has to be included in the EDF calculations in order to reproduce the correct ordering of the 2_2^+ and 0_2^+ states. In addition, it suggests an increasing prolate deformation with increasing spin number for the ground-state band, i.e., considerable centrifugal stretching, but oblate-triaxial configurations for the 0_2^+, 2_2^+, and 4_2^+ states.

ACKNOWLEDGMENTS

This experiment was supported by the BMBF (06DA9036I, 06DA9041I, 06DA7046, 06MT238, 06MT9156, 06ML234, 06KY205I, 06KY9136I), RII3-EURONS (Contract No. 506065), HIC for FAIR, Grants-in-Aid for Young Scientists (20740127) from JSPS, the SPIRE Field 5 from MEXT (Japan), and the MINIBALL and ISOLDE Collaborations.

[1] R. F. Casten, *Nuclear Structure from a Simple Perspective* (Oxford University Press, Oxford, 2000).
[2] W. R. Phillips, I. Ahmad, H. Emling, R. Holzmann, R. V. F. Janssens, T. L. Khoo, and M. W. Drigert, Phys. Rev. Lett. **57**, 3257 (1986).
[3] P. A. Butler and W. Nazarewicz, Rev. Mod. Phys. **68**, 2 (1996).
[4] N. Shimizu, T. Otsuka, T. Mizusaki, and M. Honma, Phys. Rev. Lett. **86**, 1171 (2001).
[5] P. Ring and P. Schuck, *The Nuclear Many-Body Problem* (Springer Verlag, Berlin, 1980).
[6] B. Castel and I. S. Towner, *Modern Theories of Nuclear Moments* (Clarendon, Oxford, 1990).
[7] G. Neyens, Rep. Prog. Phys. **66**, 633 (2003); **66**, 1251 (2003).
[8] J. de Boer *et al.*, Phys. Rev. Lett. **14**, 564 (1965).
[9] A. M. Hurst *et al.*, Phys. Rev. Lett. **98**, 072501 (2007).
[10] J. Ljungvall *et al.*, Phys. Rev. Lett. **100**, 102502 (2008).
[11] H. Mach, R. L. Gill, and M. Moszynski, Nucl. Instrum. Methods Phys. Res. A **280**, 49 (1989).
[12] A. Ekstrom *et al.*, Phys. Rev. C **80**, 054302 (2009).
[13] P. Reiter *et al.*, Nucl. Phys. A **701**, 209 (2002).
[14] A. Ostrowski *et al.*, Nucl. Instrum. Methods Phys. Res. A **480**, 448 (2002).
[15] J. C. Wells and N. R. Johnson, computer code LINESHAPE, ORNL, 1994.
[16] A. Jungclaus *et al.*, Phys. Lett. B **695**, 110 (2011).
[17] C. Stahl (unpublished).
[18] R. G. Helmer and M. A. Lee, Nucl. Instrum. Methods Phys. Res. **178**, 499 (1980).
[19] S. Agostinelli *et al.*, Nucl. Instrum. Methods Phys. Res. A **506**, 250 (2003).
[20] Physics Reference Manual, GEANT version 4.9.4, http://geant4.web.cern.ch/geant4/support/userdocuments.shtml.
[21] International Commission on Radiation Units and Measurements, ICRU Report No. 73 [J. ICRU **5**, No. 1 (2005)].
[22] International Commission on Radiation Units and Measurements, ICRU Report No. 49, 1993 (unpublished).
[23] H. Ower, computer programs CLX and DCY.
[24] P. Paradis *et al.*, Phys. Rev. C **14**, 835 (1976).
[25] M. Zielinska (private communication).
[26] R. D. Larsen, J. A. Thomson, R. G. Kerr, R. P. Scharenberg, and W. R. Lutz, Nucl. Phys. A **195**, 119 (1972).

[27] D. C. Radford *et al*., Phys. Rev. Lett. **88**, 222501 (2002).
[28] J. Terasaki, J. Engel, W. Nazarewicz, and M. Stoitsov, Phys. Rev. C **66**, 054313 (2002).
[29] J. Decharge and D. Gogny, Phys. Rev. C **21**, 1568 (1980).
[30] M. Bender, P.-H. Heenen, and P.-G. Reinhard, Rev. Mod. Phys. **75**, 121 (2003).
[31] T. R. Rodríguez and J. L. Egido, Phys. Rev. C **81**, 064323 (2010).
[32] J. L. Egido and L. M. Robledo, Nucl. Phys. A **518**, 475 (1990).
[33] L. M. Robledo, M. Baldo, P. Schuck, and X. Vinas, Phys. Rev. C **81**, 034315 (2010).
[34] V. Martin and L. M. Robledo, Phys. Rev. C **49**, 188 (1994).
[35] H. Zdunczuk, W. Satula, J. Dobaczewski, and M. Kosmulski, Phys. Rev. C **76**, 044304 (2007).
[36] J. L. Egido and L. M. Robledo, in *Extended Density Functionals in Nuclear Structure Physics*, edited by G. A. Lalazissis, P. Ring, and D. Vretenar, Lecture Notes in Physics Vol. 641 (Springer-Verlag, Heidelberg, 2004), p. 269.
[37] Evaluated Nuclear Structure Data File, http://www.nndc.bnl.gov/ensdf/.